JOURNAL OF GEOPHYSICAL RESEARCH, VOL. 101, NO. D7, PAGES 12,555–12,566, MAY 20, 1996

Interpretation of nitric oxide profile observed in January 1992 over Kiruna

Y. Kondo,[1] S. R. Kawa,[2] D. Lary,[3] T. Sugita,[1] Anne R. Douglass,[2] E. Lutman,[3] M. Koike,[1] and T. Deshler[4]

Abstract. NO mixing ratios measured from Kiruna (68°N, 20°E), Sweden, on January 22, 1992, revealed values much smaller than those observed at midlatitude near equinox and had a sharper vertical gradient around 25 km. Location of the measurements was close to the terminator and near the edge of the polar vortex, which is highly distorted from concentric flow by strong planetary wave activities. These conditions necessitate accurate calculation, properly taking into account the transport and photochemical processes, in order to quantitatively explain the observed NO profile. A three-dimensional chemistry and transport model (CTM) and a trajectory model (TM) were used to interpret the profile observations within their larger spatial, temporal, and chemical context. The NO_y profile calculated by the CTM is in good agreement with that observed on January 31, 1992. In addition, model NO_y profiles show small variabilities depending on latitudes, and they change little between January 22 and 31. The TM uses the observed NO_y values. The NO values calculated by the CTM and TM agree with observations up to 27 km. Between 20 and 27 km the NO values calculated by the trajectory model including only gas phase chemistry are much larger than those including heterogeneous chemistry, indicating that NO mixing ratios were reduced significantly by heterogeneous chemistry on sulfuric acid aerosols. Very little sunlight to generate NO_x from HNO_3 was available, also causing the very low NO values. The good agreement between the observed and modeled NO profiles indicates that models can reproduce the photochemical and transport processes in the region where NO values have a sharp horizontal gradient. Moreover, CTM and TM model results show that even when the NO_y gradients are weak, the model NO depends upon accurate calculation of the transport and insolation for several days.

1. Introduction

Reactive nitrogen plays important roles in the chemistry that leads to ozone (O_3) losses in the winter Arctic stratosphere. The sum of reactive nitrogen is defined as NO_y.

$$NO_y = NO + NO_2 + NO_3 + 2N_2O_5 + HNO_3 + HO_2NO_2 + ClONO_2 + BrONO_2 + \text{aerosol nitrate}$$

Active nitrogen NO_x (NO, NO_2) sequesters active chlorine by the reaction

$$\text{(R1)} \qquad ClO + NO_2 + M \rightarrow ClONO_2 + M$$

resulting in the effective reduction in the O_3 loss rates by catalytic cycles involving active chlorine. The main source of NO_2 in the lower stratosphere in the Arctic winter and spring is the photolysis of HNO_3, which constitutes the major fraction of NO_y.

NO_x is oxidized into HNO_3 indirectly via N_2O_5 and $ClONO_2$ on the surface of sulfuric acid aerosols through the following heterogeneous reactions:

$$\text{(R2)} \qquad N_2O_5 + H_2O \rightarrow 2HNO_3 \qquad \gamma_2$$

$$\text{(R3)} \qquad ClONO_2 + H_2O \rightarrow HOCl + HNO_3 \qquad \gamma_3$$

where γ_2 and γ_3 are reaction probabilities for (R2) and (R3).

The importance of (R2) at high latitudes in winter was first proposed by *Evans et al.* [1985], although the reliable reaction rate constant was not available at that time. Laboratory experiments showed that the reaction (R2) is insensitive to the composition of aerosols and particle size [*Hanson and Ravishankara*, 1991; *Fried et al.*, 1994] and slightly dependent on temperature [*DeMore et al.*, 1994]. On the other hand, (R3) becomes important only at low temperatures typical for polar winter [*Hanson et al.*, 1994, and references therein]. Attempts were made to quantitatively test the role of (R2) by the in situ measurements of reactive nitrogen on board the ER 2 aircraft at midlatitudes [*Fahey et al.*, 1993; *Kawa et al.*, 1993]. They showed the importance of (R2) in controlling the NO_x/NO_y ratio in the lower stratosphere at midlatitude under background and volcanic aerosols conditions.

Compared with midlatitudes, high-latitude winter is characterized by short daylight hours and lower temperatures. These conditions can change the importance of heterogeneous effects compared with midlatitudes. Low insolation especially reduces aerosol surface area (SA) required to effectively lower the NO_x/NO_y ratio as expected from the calculation by *Mills et al.* [1993]. NO mixing ratios were observed up to 30.5 km from

[1]Solar-Terrestrial Environment Laboratory, Nagoya University, Toyokawa, Japan.
[2]NASA Goddard Space Flight Center, Greenbelt, Maryland.
[3]Department of Chemistry, University of Cambridge, Cambridge, England.
[4]Department of Atmospheric Science, University of Wyoming, Laramie.

Paper number 96JD00578.
0148-0227/96/96JD-00578$09.00

Table 1. Balloon Measurements From Kiruna on January 22 and 31, 1992

Date	Species	Method	Investigator
	January 22, 1992		
Ascent and descent	NO	chemiluminescence	Y. Kondo
Ascent	O_3	ECC	Y. Kondo
Ascent	aerosol	particle counter	Y. Kondo
Descent	N_2O	grab sampler	U. Schmidt
Ascent and descent	actinic flux	filter radiometer	C. Schiller
	January 31, 1992		
Ascent	NO_y	chemiluminescence	Y. Kondo
Ascent	O_3	ECC	Y. Kondo
Descent	N_2O	grab sampler	U. Schmidt

ECC, electrochemical cell.

Table 2. Solar Zenith Angle During Ascent of the Balloon on January 22, 1992

Pressure, hPa	Altitude, km	SZA, deg	PT, K
84.4	16.7	91.0	420
59.4	18.8	90.5	450
40.2	21.1	90.0	492
24.9	23.8	89.5	554
17.5	25.8	89.0	625
15.9	26.4	88.8	650
12.0	28.0	88.5	717
9.9	29.2	88.2	800
8.6	30.1	88.0	857

Abbreviations are SZA, solar zenith angle, and PT, potential temperature.

Kiruna (68°N, 20°E), Sweden, on January 22, 1992 [*Aimedieu et al.*, 1994]. The NO values up to 25 km were extremely low, as compared with those observed at midlatitude in fall [e.g., *Kondo et al.*, 1989; Y. Kondo et al., The effect of Pinatubo aerosols on stratospheric NO, submitted to *Journal of Geophysical Research*, 1996 (hereinafter referred to as Y. Kondo et al., submitted manuscript, 1996)]. Since Kiruna was located near the terminator and edge of the polar vortex, quantitative interpretation of the observed NO profile requires accurate evaluation of the chemical and transport processes controlling the abundance of active nitrogen. For this purpose, partitioning of NO_y was calculated by models which take into account the photochemistry and transport processes. The comparison shows the capability of the current models in accurately predicting the NO which has a large spatial gradient and undergoes rapid temporal changes due to large variations in the photolysis rates controlling the NO levels.

2. Data Set

2.1. Balloon Data

Balloon-borne measurements of NO, O_3, N_2O, aerosol, and actinic solar flux up to 30.5 km (8.2 hPa) were made from Kiruna (68°N, 20°E), Sweden, on January 22, 1992, as a part of the European Arctic Stratospheric Ozone Experiment (EASOE) [*Aimedieu et al.*, 1994; *Bauer et al.*, 1994; *Schiller et al.*, 1994]. Similarly, NO_y, O_3, N_2O, and aerosol were measured on January 31 [*Kondo et al.*, 1994; *Bauer et al.*, 1994]. The species measured on these days are summarized in Table 1. Most of the experimental data used in the present paper were already given in the papers cited above. In this paper we focus on the quantitative interpretation of the NO profile using these data. Some additional data closely relevant to the present work are given below, with brief summaries of the instruments and accuracies of the measurements.

January 22. NO was measured with a chemiluminescence detector [*Kondo et al.*, 1988] during ascent between 0720 and 0930 UT and also during part of the descent, which was made about 2.5 hours after the ascent. The solar zenith angle (SZA) during ascent is given in Table 2. The SZA during descent was 87.8° ± 0.3°. The accuracy and the detection limit for the NO values averaged for 10 s are about 10% and 15 parts per trillion by volume (pptv), respectively, between 20 and 32 km [*Kondo et al.*, 1988, 1989].

The NO values during descent were somewhat larger than those during ascent probably in part due to the diurnal variation of NO. However, there is, of course, a rapid variation in NO near the terminator. The measured NO values were generally lower than 50 pptv below 23 km. At 26 km the NO mixing ratio was still as low as 100 pptv. These NO values were an order of magnitude smaller than those measured at midlatitudes in fall [e.g., *Kondo et al.*, 1989, also submitted manuscript, 1996]. The NO mixing ratio started to increase rapidly at around 26 km. A low NO mixing ratio was also observed below 27 km near 50°N in winter by *Ridley et al.* [1984, 1987].

O_3 was measured with an electrochemical concentration cell (ECC) sonde during ascent with an uncertainty of 2–10% between 15 and 30 km [*Komhyr et al.*, 1995] and is shown in Figure 1. N_2O measurements were made by collecting air samples during the parachute descent of the gondola, followed by gas chromatographic analysis in the laboratory [*Bauer et al.*,

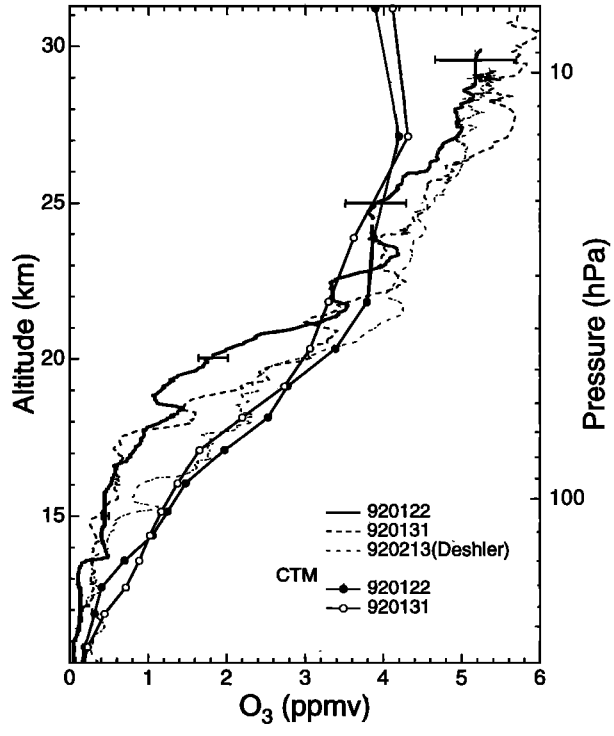

Figure 1. The O_3 profiles measured during ascent on January 22, January 31, and February 13, 1992. Bars indicate the uncertainty of the measurements. O_3 profiles calculated by the chemistry and transport model (CTM) for January 22 and 31 are also shown.

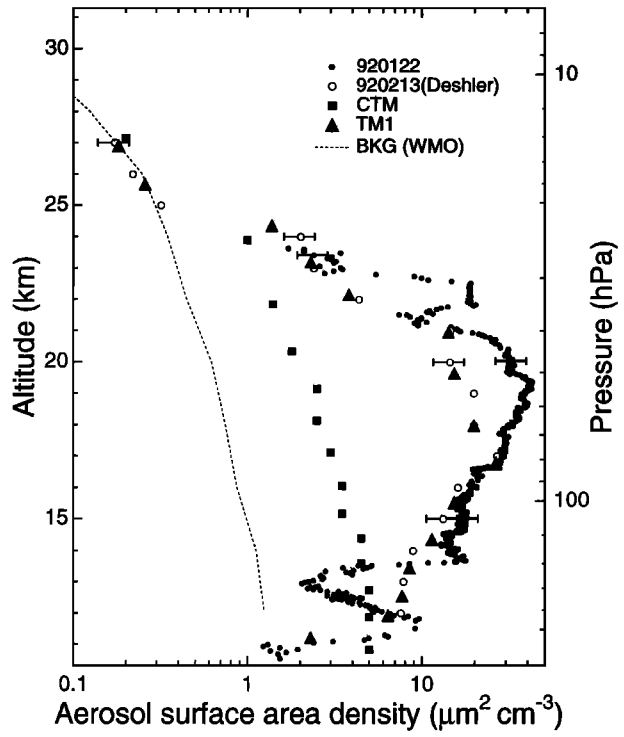

Figure 2. Profiles of aerosol surface area (SA) measured from Kiruna on January 22, 1992 (solid circles), and February 13, 1992 (open circles). The SA used for CTM are shown as squares. Typical background SA (BKG) is shown as a dashed line.

1994]. The uncertainty of the measurement is ±10% above 24 km and less than ±5% at lower altitudes.

Aerosol concentrations were measured with an optical particle counter [*Aimedieu et al.*, 1994]. A detailed description of the instrument is given by T. Sugita et al. (manuscript in preparation, 1996). Concentrations of aerosols with radii larger than 0.23, 0.28, 0.31, 0.41, 0.58, 2.0, and 3.3 μm were measured. The detection limit was 1.4×10^{-3} cm^{-3}. Concentrations of aerosols with radii larger than 2.0 μm were below the detection limit in the stratosphere. SA was calculated from the measured aerosol size distribution, and the ascent profile is shown in Figure 2. The SA for a typical nonvolcanic period as given by *World Meteorological Organization* (*WMO*) [1992, Table 8-8] is also shown for reference. The observed SA was much larger than the background value owing to the Pinatubo volcanic aerosols.

The observed temperature shown by *Aimedieu et al.* [1994] was the lowest between 21 and 24 km, barely reaching the nitric acid trihydrate (NAT) condensation temperature, which was calculated following the formulation by *Hanson and Mauersberger* [1988]. Considering that in the Arctic, polar stratospheric clouds (PSC) are often only observed at relatively high supersaturation [*Kawa et al.*, 1992; *Kondo et al.*, 1992], the observed particles on January 22 can be considered to be composed of sulfuric acid and water.

For reference, SA estimated from the aerosol concentrations measured by *Deshler* [1994] over Kiruna on February 13, 1992, are also shown in Figure 2. Condensation nuclei and aerosols with radii larger than 0.15, 0.25, 0.48, 1.08, 1.93, 2.76, 4.74, and 9.50 μm were measured. Above 24 km, aerosols with radii smaller than 0.15 μm made the major contribution to SA [*Deshler*, 1994]. Since the smallest size of the aerosols measured on January 22 was 0.23 μm, SA estimated from measurements of aerosols larger than this size can be significantly underestimated above 24 km and are therefore not shown here.

SA observed on January 22 and February 13 agrees reasonably well below 23 km, as shown in Figure 2. Kiruna was located outside the vortex at 475 K (20 km) and at the inner edge at 550 K (23 km) on January 22, as discussed below. The potential vorticity (PV) value over Kiruna at 550 K on February 13 was 126×10^{-6} K m^2 kg^{-1} s^{-1}, which is similar or even somewhat larger than the value on January 22 as given in Table 3. The similar aerosol profiles on these two days are consistent with the similarities in the location of the vortex boundary relative to Kiruna. The O_3 profile observed on February 13 is shown in Figure 1 for comparison. The O_3 profile on February 13 agrees well with that on January 22 above 22 km. It has been found that correlation between SA and O_3 above 16 km changed significantly depending on the location of measurements relative to the vortex boundary [*Borrmann et al.*, 1995]. Considering the agreement of the PV and O_3 values on February 13 with those on January 22, SA from *Deshler* [1994] may be considered to give a reasonable estimate for January 22 above 23 km.

NO_2 photodissociation coefficient ($J(NO_2)$) has been derived from the UV flux measurements made simultaneously (C. Schiller, unpublished data, 1996). The radiometer used to measure the UV flux is described by *Schiller et al.* [1994]. During ascent, SZA was larger than 89° below 22 km. In this altitude region, $J(NO_2)$ was significantly reduced owing to increased optical thickness caused by the enhanced aerosol loading as shown in Figure 2. This gives no impact to the present analysis because comparisons of model values with NO values obtained during ascent are made only above 24 km.

Table 3. Potential Vorticity Values at Various Potential Temperatures at Kiruna

PT, K	Pressure, hPa	Approximate Altitude, km	PV Jan. 22, 10^{-6} K m^2 kg^{-1} s^{-1}	In/Out	PV Jan. 31, 10^{-6} K m^2 kg^{-1} s^{-1}	In/Out
350	140	13	6	...	6	...
380	120	14	9	out	7	out
400	100	16	10	out	9	out
475	46	20	24	out	33	edge
550	25	23	102	in/edge	108	in/edge
650	16	26	144	in	129	in
700	13	27	190	in	170	in
800	10	29	284	in	250	in

Abbreviations are PV, potential vorticity, and PT, potential temperature.

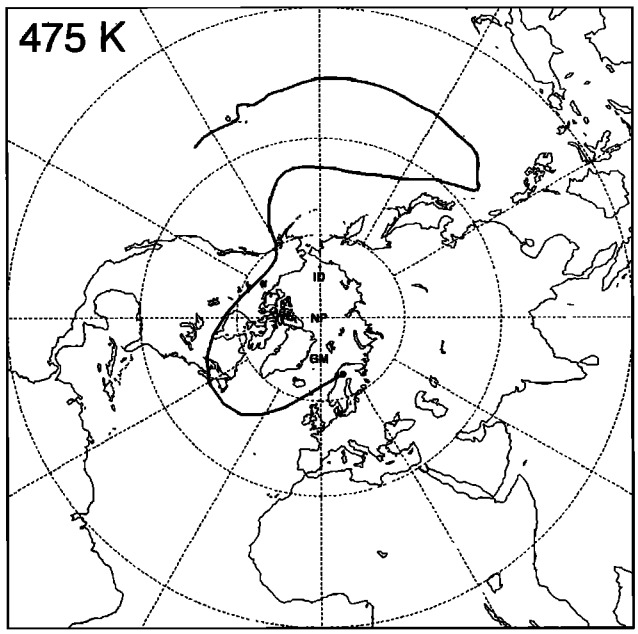

Figure 3a. Isentropic trajectories arriving over Kiruna on January 22, 1992, on isentropic level of 475 K.

January 31. NO_y was measured with a chemiluminescence NO detector combined with a gold catalytic converter heated at 300° ± 1°C, as described in detail by *Kondo et al.* [1990, 1992]. The overall error is estimated to be ±15% between 15 and 31 km. O_3 was measured with an ECC sonde during ascent and is shown in Figure 1.

2.2. Meteorological Data

Maps of Ertel's potential vorticity (PV) at six potential temperature surfaces of 350 K (13 km), 380 K (14 km), 400 K (16 km), 475 K (20 km), 550 K (23 km), and 700 K (27 km) were provided by the European Center for Medium-Range Weather Forecasts (ECMWF). The PV values at 800 K were calculated using the same meteorological data as used for the chemistry transport model which is described below. The vortex boundary at 475, 550, and 700 K was defined as the region with PV values of $40 \pm 8 \times 10^{-6}$, $90 \pm 12 \times 10^{-6}$, and $160 \pm 20 \times 10^{-6}$ K m^2 kg^{-1} s^{-1}, respectively. PV values at these potential temperatures over Kiruna on January 22 and 31 are given in Table 3. They were 24, 102, and 190 $\times 10^{-6}$ K m^2 kg^{-1} s^{-1} at 475, 550, and 700 K, respectively, on January 22. The PV maps indicate that Kiruna was located outside the vortex below 475 K, at the inner edge of it at 550 K, and inside it at 700 and 800 K. On January 31 the location of Kiruna relative to the vortex boundary was similar to January 22.

Isentropic 30-day back trajectories were calculated from United Kingdom Meteorological Office analyses. The trajectories used in this study were for January 22, 1992, and finished over Kiruna. The trajectories at the 475- and 550-K levels are shown in Figures 3a and 3b, respectively. The air parcels below 475 K originate from lower latitudes, while they remain in high latitudes at 550–1000 K, corresponding to the PV analysis as mentioned above.

3. Models

3.1. Chemical Scheme

At night, NO_x is oxidized into N_2O_5 via the following reactions:

(R4) $NO_2 + O_3 \rightarrow NO_3 + O_2$

(R5) $NO_2 + NO_3 + M \rightarrow N_2O_5 + M$

NO_x is also sequestered as $ClONO_2$ via (R1). N_2O_5 and $ClONO_2$ are photolized back to NO_x with time constants of from several hours to a few days, depending on altitude and SZA.

(R6) $N_2O_5 + h\nu \rightarrow NO_2 + NO_3$

(R7) $ClONO_2 + h\nu \rightarrow Cl + NO_3$

Further oxidation of N_2O_5 and $ClONO_2$ into HNO_3 occurs by the heterogeneous reactions (R2) and (R3). Photolysis or the reaction with OH reproduces NO_x from HNO_3 with a time constant of a few weeks or less.

(R8) $HNO_3 + h\nu \rightarrow NO_2 + OH$

(R9) $HNO_3 + OH \rightarrow NO_3 + H_2O$

In order to quantitatively evaluate critical processes in controlling NO_x levels in the Arctic winter in combination with transport processes, the NASA Goddard Space Flight Center (GSFC) three-dimensional (3-D) chemistry and transport model (CTM) and trajectory models from NASA GSFC and the University of Cambridge were used. Descriptions of these are given below.

3.2. Chemistry and Transport Model (CTM)

A meteorological data assimilation [*Schubert et al.*, 1993] was used to produce winds and temperatures that drove the off-line 3-D chemistry and transport model. In the assimilation, fields for winds and temperatures which satisfy the equations of motion are produced from combination of a general circulation model and observations. Constituent fields calculated with a CTM using these observation-based winds and temperatures may be compared directly with constituent observations. Constituents in the CTM were initialized November 15, 1991, with

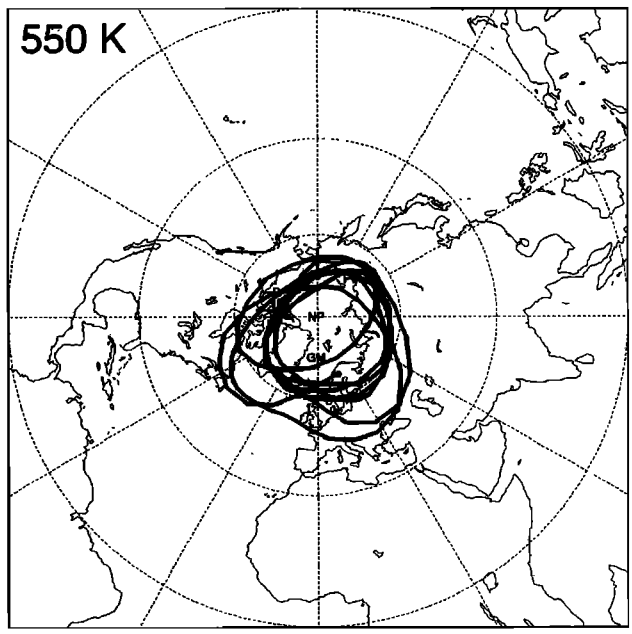

Figure 3b. Same as Figure 3a but for the 550-K level.

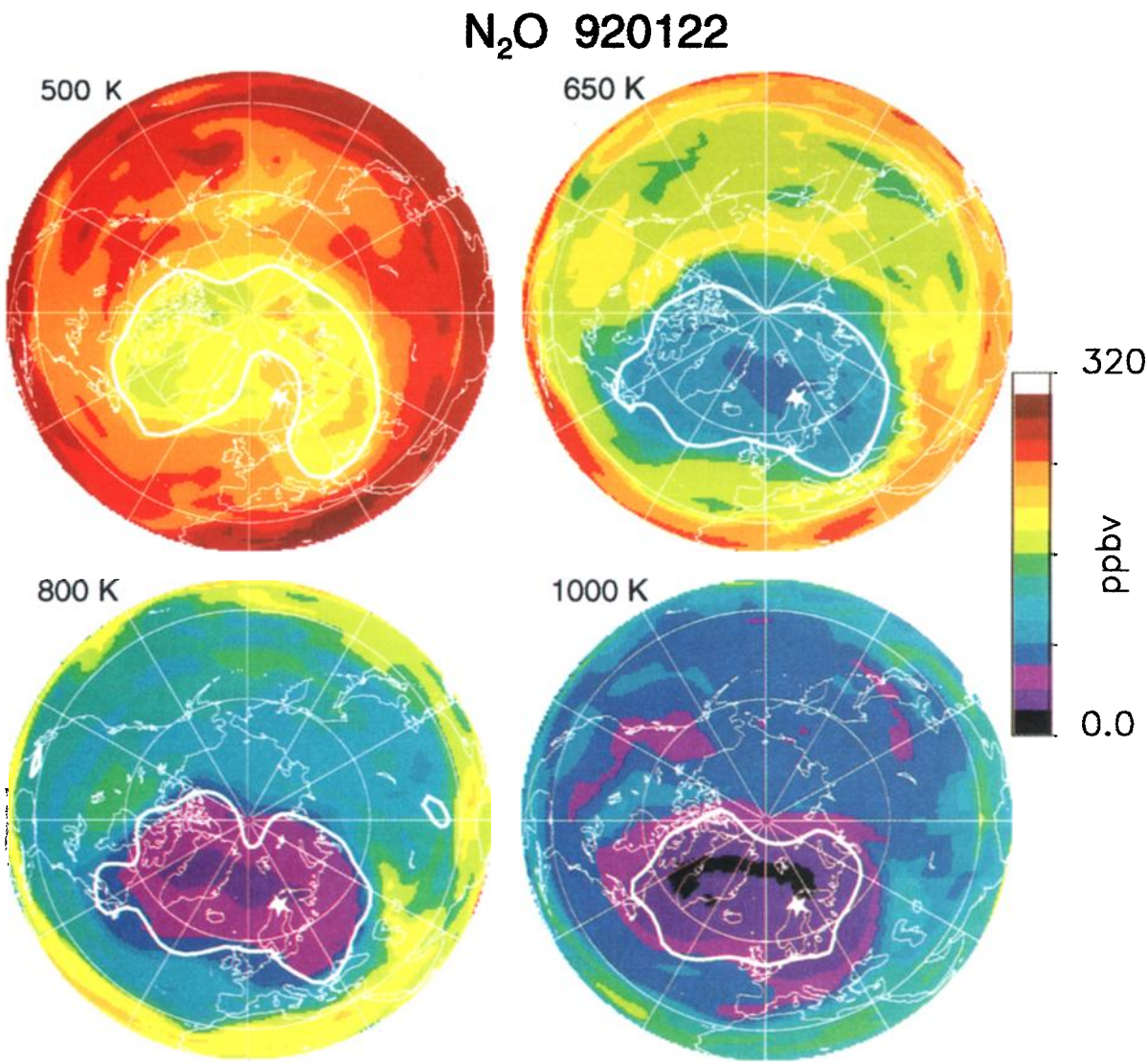

Plate 1a. Maps of N_2O calculated by CTM for January 22, 1992, at isentropic levels of 500, 650, 800, and 1000 K. The vortex boundary is indicated as a white line. The location of Kiruna is denoted with a star.

O_3 data from microwave limb sounder (MLS), N_2O from cryogenic limb array etalon spectrometer (CLAES) on upper atmosphere research satellite (UARS), and results from a two-dimensional model. The CTM ran with a horizontal resolution of 2° in latitude and 2.5° in longitude with 15-min time steps. Mixing ratios of 34 species are calculated at 25 pressure levels between 0.63 and 922 hPa.

Equatorward of 60°N, the Stratospheric Aerosol and Gas Experiment II (SAGE II) satellite experiment SA data was used [*Thomason and Poole*, 1993]. The SA north of 60°N was chosen from the data given in chapter 8 of *WMO* [1992], and the adopted profile is shown in Figure 2. This SA represents the enhanced value. As can be seen from Figure 2, the SA values used in this model are similar to those obtained by in situ measurements at 24 and 27 km. The model SA values are much lower than measured values below 24 km. However, it has been found from simple calculation that the partitioning of the reactive nitrogen depends little on the SA values exceeding 1 μm^2 cm^{-3} under Arctic winter conditions due to saturation of the heterogeneous reaction on sulfuric acid aerosol as observed in midlatitudes [*Fahey et al.*, 1993; *Mills et al.*, 1993].

Photolysis in the CTM uses a look-up table based on the radiative transfer model of *Anderson and Lloyd* [1990] and *Anderson et al.* [1995] with molecular cross sections from *DeMore et al.* [1992]. The calculations assume clear sky and a uniform surface albedo of 0.3. Absorption by overhead ozone depends on the model O_3 profile.

3.3. Trajectory Models

TM1. The 10-day back trajectories from Kiruna on January 22 were calculated on 20 isentropic levels between 330 and 1000 K using the same wind and temperature fields as used for CTM. The vertical resolution is about 1.5 km above 20 km. Changes in the partitioning of reactive nitrogen were calculated along these trajectories including the same chemical reactions as used for CTM. The O_3 and NO_y mixing ratios obtained by the balloon observations were used. The SA used by the model was taken from the in situ measurements up to 27 km as shown in Figure 2.

TM2. The trajectory model used in this study was a version of a new suite of models called AUTOCHEM. A total of 62 species were included. No family or photochemical equilibrium

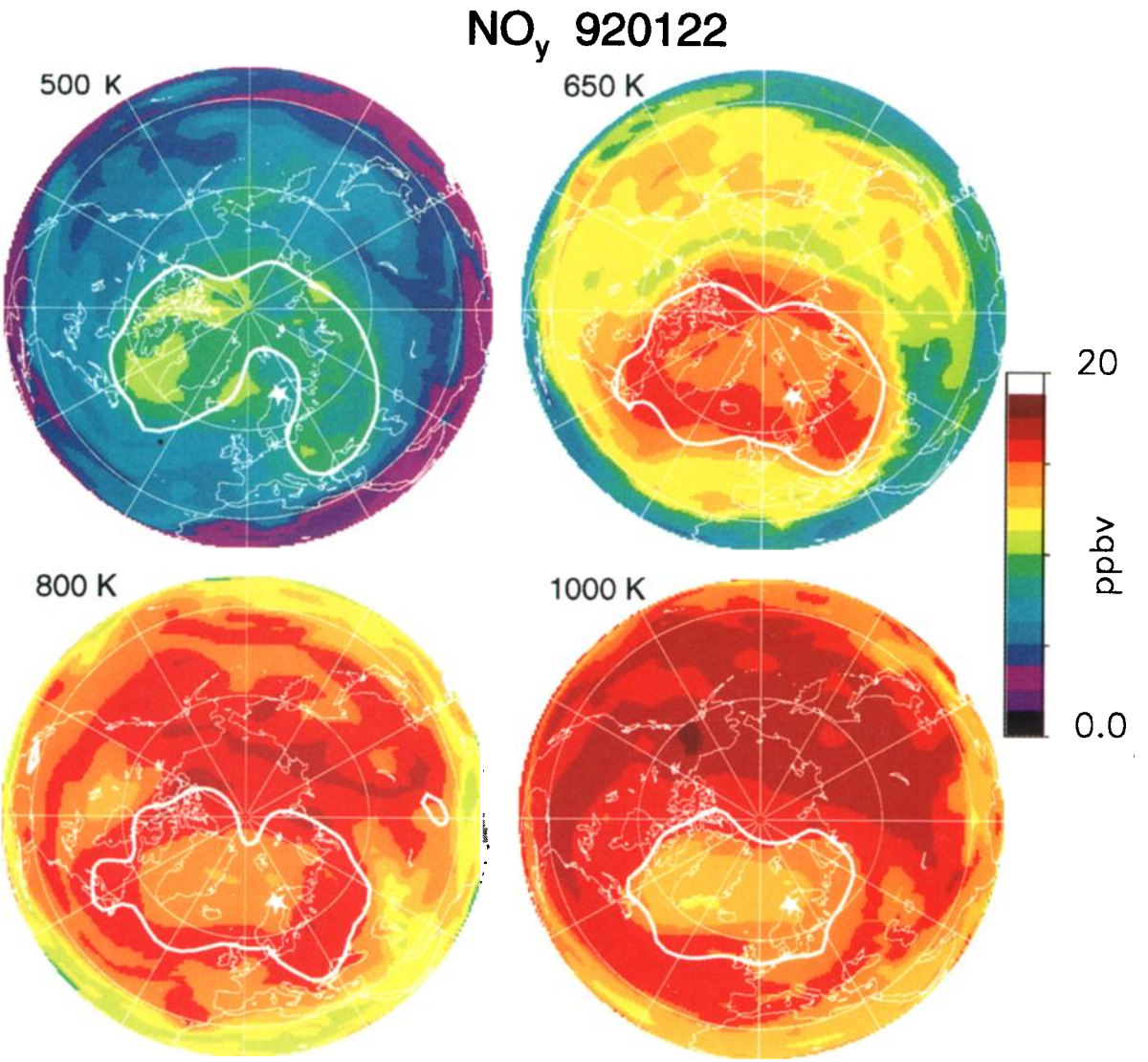

Plate 1b. Same as Plate 1a but for NO_y.

assumptions were made. Sixty species, including reactive nitrogen, hydrogen, chlorine, and bromine species, were integrated separately with a 15-min time step. The version of AUTOCHEM used in this study contained a total of 292 reactions, 170 bimolecular reactions, 37 trimolecular reactions, 47 photochemical reactions, and 38 heterogeneous reactions on PSC and sulfate aerosol. The rate constants for the reactions were taken from *Atkinson et al.* [1992] and *DeMore et al.* [1994]. Photolysis rates were calculated using full spherical geometry and multiple scattering as described by *Lary and Pyle* [1991] after *Meier et al.* [1982], *Nicolet et al.* [1982], and *Anderson* [1983].

The isentropic trajectory model calculations were performed to simulate the chemical composition of air parcels arriving over Kiruna on January 22. The values used for NO_y, O_3, and SA are the same as for TM1. The partitioning of reactive nitrogen at the start of the simulation, together with all the other constituent concentrations, was taken from a January simulation of the Cambridge two-dimensional model [*Harwood and Pyle*, 1977, 1980].

4. Comparison with Models

4.1. Chemical Fields

In order to understand the location of Kiruna in the chemical fields, hemispheric plots of N_2O, NO_y, NO_x, and NO on the 500, 650, 800, and 1000 K calculated from the CTM are shown in Plates 1a–1d for January 22. For reference the boundary of the polar vortex is shown as a white line. The boundary was determined from PV gradients [*Nash et al.*, 1996].

The modeled N_2O values inside the vortex are smaller than those outside at 500 and 650 K. This is due mainly to stronger descent by diabatic cooling inside the vortex. The gradient of N_2O through the vortex boundary is also caused by inefficient horizontal transport of N_2O from lower latitude to inside the vortex. Corresponding to the N_2O distribution, NO_y, values inside the vortex are larger than those outside it at 500 and 650 K. However, at 800 and 1000 K, NO_y values inside the vortex are slightly smaller than outside it. As shown below, NO_y decreases with altitude above 26 km due to net loss of NO_y

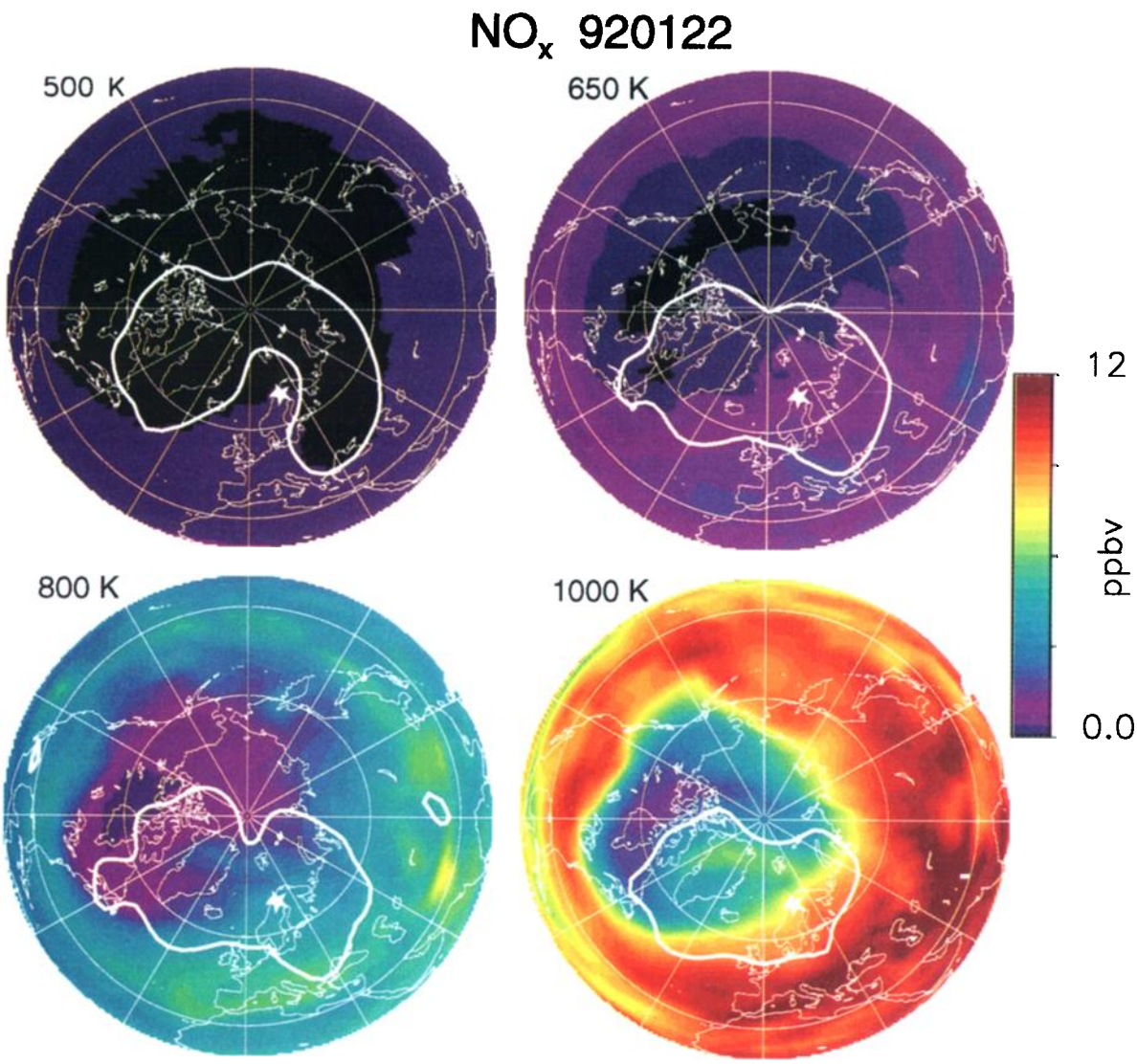

Plate 1c. Same as Plate 1a but for NO_x.

through the reaction $N + NO \rightarrow N_2 + O$ in the tropical upper stratosphere. Stronger descent inside the vortex brings down air poorer in NO_y from above, causing smaller NO_y values at 800 and 1000 K.

In contrast, large gradients in NO_x and NO are not defined by the vortex boundary, as can be seen from Plates 1c and 1d. The NO_x/NO_y ratio is controlled by the conversion of NO_x to N_2O_5 and further oxidation into HNO_3 and the photolysis of these reservoir species. Here γ_3 calculated based on the results by *Hanson and Ravishankara* [1991] reaches the maximum value of 0.01 at 23 km where temperature was the lowest. Since γ_2 is 0.1, the γ_3/γ_2 ratio does not exceed 0.1. Above 25 km and below 20 km the γ_3/γ_2 ratio is lower than 0.04. Therefore (R2) plays a dominant role in oxidizing NO_x.

The time constants of the photolysis of N_2O_5 and HNO_3 vary from several days to a few weeks, depending on altitude and SZA. Therefore the NO_x/NO_y ratio depends on the time history of air parcels over the last few days. On the other hand, NO is in almost immediate photochemical equilibrium with NO_2. Therefore the NO/NO_x ratio is controlled by the instantaneous solar illumination, temperature, and O_3 concentration. Plate 1d clearly shows strong control of insolation on NO. Because of the complex distribution of the NO/NO_y ratio, interpretation of the NO profile measured at Kiruna requires models which adequately take into account photochemical and transport processes.

The profiles of O_3 observed on January 22 and 31 are compared with those constructed from the CTM for the same location (68°N, 20°E) and dates in Figure 1. Modeled O_3 values agree well with the measured values between 21 and 27 km. However, below 20 km the model significantly overestimates the O_3 abundance. On the other hand, at 31 km the calculated O_3 value is 20–30% lower than that observed. The discrepancy below 20 km is not relevant to the present discussion, since detailed comparison of the observed and calculated NO values are made above 20 km. The effect of the O_3 difference at 31 km is discussed below.

The profiles of N_2O observed on January 22 and 31 are compared with those calculated by the model in Figure 4. Modeled N_2O values agree well with the measured values up to 22 km. However, at higher altitudes the model overestimates the N_2O abundance. The observed N_2O mixing ratios as low as 10–20 parts per billion by volume (ppbv) are caused by strong descending motion inside the vortex induced by diabatic

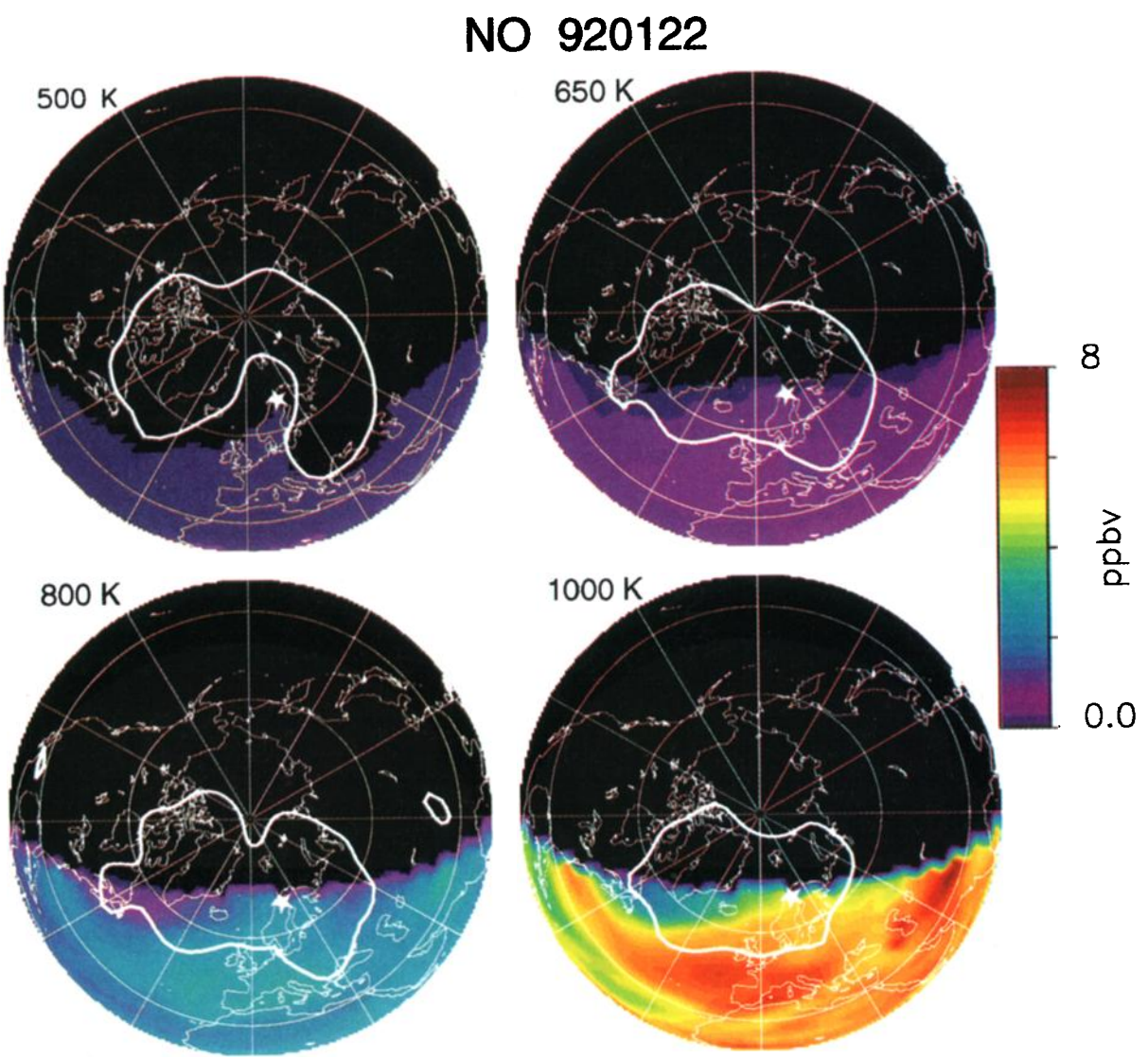

Plate 1d. Same as Plate 1a but for NO.

cooling [*Bauer et al.*, 1994]. It is indicated that the descending process is not well reproduced in the assimilation wind fields.

The model NO_y profiles at 66°N and 70°N at 20°E are compared with that observed in Figure 5. The model NO_y profile at 68°N almost overlaps with that at 70°N above 17 km and hence is not plotted here. For reference, the model NO_y profile at 68°N on January 22 is also shown. Generally, the model NO_y for 68°N and January 31 agrees well with the observed one. The agreement is especially good below 23 km. This is consistent with the comparison of N_2O as discussed above, considering that N_2O and NO_y are tightly correlated in the lower stratosphere [*Fahey et al.*, 1990; *Loewenstein et al.*, 1993; *Kondo et al.*, 1994]. Even above 22 km, difference between the model and measurements is not so large as for N_2O. This is because NO_y mixing ratios do not increase linearly with the decrease in N_2O for N_2O mixing ratio lower than 100 ppbv [*Loewenstein et al.*, 1993; *Kondo et al.*, 1994], as NO_y is subject to photochemical loss at these altitudes. Because of this, the lack of the strong descent does not lead to significant underestimation of the NO_y mixing ratio by the model.

It can be seen from Figure 5 that the profiles of the modeled NO_y mixing ratio vary little with latitude between 66°N and 70°N. Correspondingly, the N_2O mixing ratios vary little with latitude, although they are not shown here. The model also predicts that the changes in the NO_y values between January 22 and 31 are small. Similarity in the N_2O profiles on these days can be seen in Figure 4.

4.2. NO Profile

The model NO profiles by CTM for 0900 and 1200 UT on January 22 are compared with the observed profiles in Figures 6 and 7. In the model the SZA at 0900 and 1200 UT are 89.1° and 88.8°, respectively. In addition, profiles of all reactive nitrogen species calculated for 1200 UT on January 22 are shown in Figure 8. The partitioning of NO_y at each level is given in Table 4. These show that NO + NO_2 is a minor component of NO_y. Considering the SZA given in Table 3, ascent data which can be used for comparison with the CTM are limited to those obtained above 24 km, where SZA was smaller than 89°. All the descent data can be used for the comparison, although the number of data points below 26 km is limited due to the high descent speed. For these data, $J(NO_2)$ was disturbed little by the Pinatubo aerosol, as discussed above.

The NO mixing ratios were calculated by TM1 on the tra-

jectories reaching Kiruna on January 22. The calculated NO profile for 0930 UT is shown in Figures 6 and 7.

The changes in the NO/NO_y ratio simulated by TM2 along the back trajectories are shown in Figure 9. The NO/NO_y ratios were also calculated including only gas phase chemistry, and these results are also shown as a reference. The NO/NO_y ratio at the start of the simulation has little influence on the results shown. Air parcels arriving at Kiruna during sunrise on January 22 on the isentropic level at 550 K had seen less sunlight than those at the other levels during the previous 10 days. This is clearly evident when examining the 10-day time series of the NO/NO_y ratio shown in Figure 9. On the 550-K isentropic surface, the most sunlight was seen on January 16 and 17. The NO profile calculated by TM2 is compared with the observations in Figures 6 and 7. In Figure 7 the NO values calculated including only gas phase chemistry are compared with those including heterogeneous chemistry.

Both CTM, TM1, and TM2 well reproduce the observed NO profile between 20 and 27 km. The good agreement between the observations and TM1 results extends up to 30 km. The calculated NO values between 19 and 22 km are lower than 40 pptv in agreement with the descent data. At this level, NO_x/NO_y and $2(N_2O_5/NO_y)$ ratios calculated by CTM are about 0.01 and 0.001, respectively (Table 4). Reaction (R2) reduces the NO_x level by more than an order of magnitude, as can be seen from Figures 7 and 9. Agreement of TM1 and TM2 with CTM, which uses less SA than TM1 and TM2, indicates saturation at low SA amounts for these trajectories. NO mixing ratio at 24 km has been calculated as a function of SA by using TM2. The NO values relative to those including only gas phase chemistry are 0.18, 0.13, 0.11, and 0.09 for SA = 0.40, 0.60, 1.0, and 2.0 $\mu m^2\ cm^{-3}$, respectively. Since background SA is 0.4–0.6 $\mu m^2\ cm^{-3}$ at 20–24 km (Figure 2), predominant reduction in NO below 24 km is predicted to occur by heterogeneous chemistry under nonvolcanic conditions. Volcanic aerosol reduces NO further by 50%.

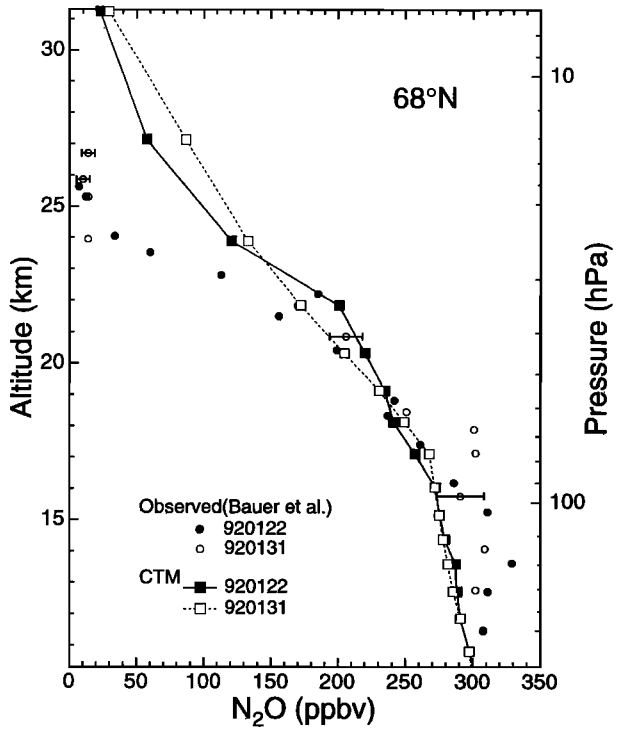

Figure 4. Comparison of the N_2O profiles observed from Kiruna on January 22 (solid circles) and January 31, 1992 (open circles), with those calculated by CTM (solid and open squares).

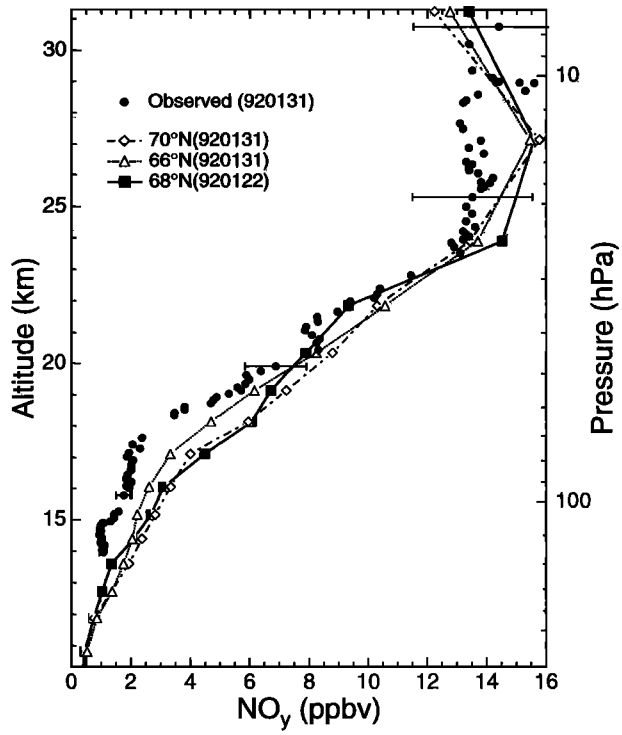

Figure 5. Comparison of the NO_y profile observed from Kiruna on January 31, 1992 (solid circles), with those calculated by CTM for 66°N (triangles) and 70°N (diamonds). The CTM results for January 22 are also shown (solid squares).

The rapid increase in the NO values between 24 and 29 km is well reproduced in the models. As can be seen from Table 4, the increase in NO in this altitude region is due to an increase in the NO_x/NO_y ratio resulting from the reduced SA (Figure 2) and increased rate of HNO_3 photolysis. The increase in the NO values above 24 km is associated with the decrease in the HNO_3 values.

The CTM model NO values at 0900 UT are somewhat smaller than those at 1200 UT between 20 and 24 km, as can be seen from Figure 7. At 24 km the NO_x mixing ratio is 80 pptv at 0900 UT, while it is 270 pptv at 1200 UT. At 0900 UT the model values of N_2O_5, HNO_3, $ClONO_2$, and HO_2NO_2 are larger than those at 1200 UT. Most of the difference in the NO_x value is balanced by the difference in the values of HNO_3 and $ClONO_2$, which are the dominant components of NO_y below 24 km, as can be seen from Figure 8. Considering the time constant of the photolysis of these reservoir species, the difference in the NO_x values between 0900 and 1200 UT is primarily caused by the diurnal variation of NO_x resulting from $ClONO_2$ photolysis. This emphasizes the importance of using a model that accurately simulates the diurnal cycle in comparing a single NO profile at this critical season and latitude.

At 31 km the CTM NO mixing ratio is 3.9 ppbv at 1200 UT. Similarly, TM2 NO values are 2.5–3.6 ppbv at 30.5 km. If these values are used to linearly interpolate model values between 27 and 31 km, the calculated NO values are considerably higher than those observed between 29 and 30.5 km, as can be seen

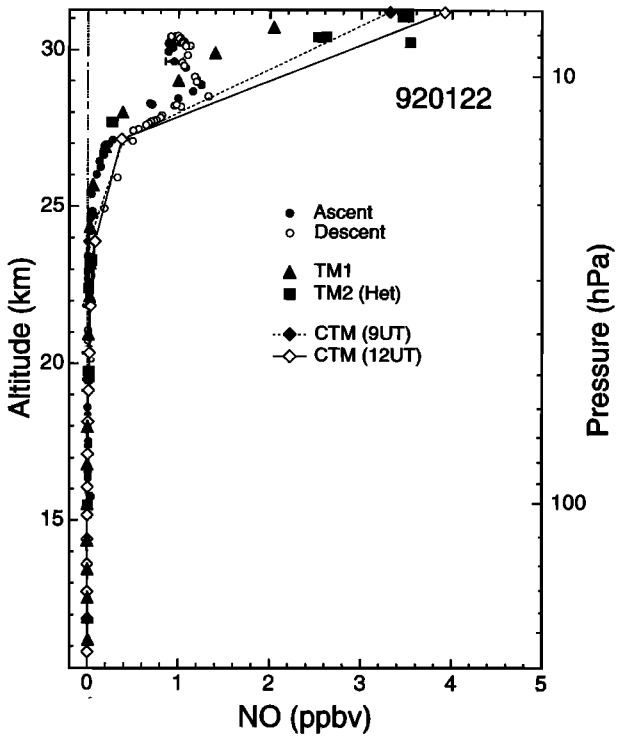

Figure 6. Comparison of the NO profile observed from Kiruna on January 22, 1992 (solid and open circles), with those calculated by CTM for 1200 UT (open diamonds) and 0900 UT (solid diamonds). The NO profile calculated by TM1 is shown as closed triangles. The TM2 values including heterogeneous chemistry (TM2(Het)) are shown as solid squares.

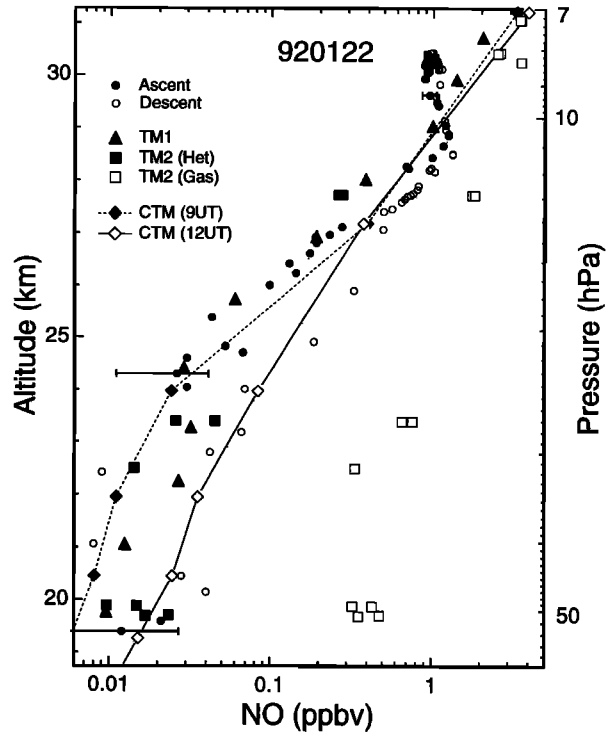

Figure 7. Same as Figure 6 but for above 19 km. The TM2 values including only gas phase chemistry (TM2(Gas)) are also shown as open squares.

from Figure 6. In contrast, the TM1 values in this altitude region are in better agreement with the observations as mentioned above. The shape of the NO vertical profile is better simulated by TM1 owing to higher vertical resolution. The O_3 mixing ratio used for TM1 around 30 km is 20–30% higher than that used by CTM. Specifying observed O_3 in TM1 decreases NO by about 15% from that using CTM O_3, indicating that the difference in the O_3 value is not the major cause of the difference between CTM and TM1.

Garcia and Solomon [1994] examined the possible effect of (R2) in the upper stratosphere, where SA and composition of aerosol are poorly known. They used SA given by *WMO* [1992] at 32 km and extrapolated it exponentially above 32 km. It has been found that in the upper stratosphere, HNO_3 mixing ratios calculated including (R2) are considerably larger than those for the gas phase case in high-latitude winter when the effect of (R2) is maximized. This effect corresponding to the conditions for our observations was calculated using CTM. The SA shown in Figure 2 was extended up logarithmically, leading to the value of 0.041 $\mu m^2\ cm^{-3}$ at 7 hPa. Over 20 days from January 2 to January 22, this reduced NO_x and N_2O_5 mixing ratios at 7 hPa by 0.8 ppbv (20%) and 0.5 ppbv (25%), respectively, from the gas phase case. On the other hand, HNO_3 increased by 1.9 ppbv (nearly 70%), and $ClONO_2$ was not significantly affected. Since the HNO_3 was still increasing after 20 days, the full effect of (R2) may be greater than these values. Since the present models do not include the effect of (R2) above 28 km, the calculated NO may be overestimated to some extent.

It can be concluded that the observations of NO made over Kiruna during sunrise on January 22 are consistent with calculations made by the CTM, TM1, and TM2. These models reproduce the observed very low NO/NO_y ratio and identify the two main reasons for this: (1) There was very little sunlight to generate NO_x from HNO_3, and (2) there was oxidation of

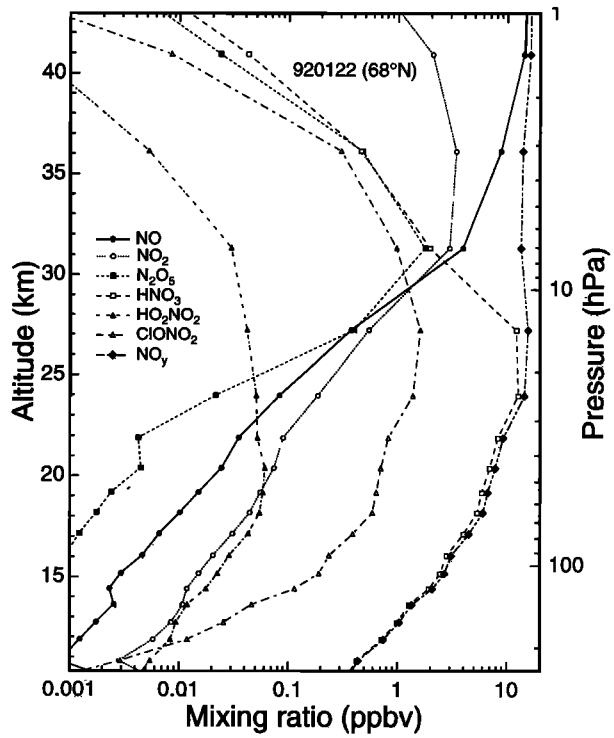

Figure 8. Profiles of each NO_y species calculated by CTM for Kiruna at 1200 UT on January 22, 1992.

Table 4. Partitioning of NO_y Calculated by the Chemistry and Transport Model for January 22, 1992

Pressure, hPa	NO_x/NO_y	$2(N_2O_5)/NO_y$	HNO_3/NO_y	HO_2NO_2/NO_y	$ClONO_2/NO_y$
92	0.008	0.0006	0.905	0.009	0.077
77	0.008	0.0005	0.893	0.010	0.088
65	0.009	0.0006	0.884	0.009	0.098
55	0.011	0.0007	0.884	0.009	0.096
45	0.013	0.0011	0.889	0.008	0.089
35	0.013	0.0009	0.891	0.006	0.089
24	0.019	0.0030	0.879	0.004	0.095
14	0.059	0.0517	0.783	0.003	0.103
7	0.514	0.264	0.147	0.002	0.073

NO_x due to hydrolysis of N_2O_5 which was particularly noticeable between 20 and 23 km.

5. Summary

CTM, TM1, and TM2 were run to simulate the profile of the mixing ratio of NO up to 30.5 km obtained by balloon-borne measurements made at 68°N in January 1992. Hemispheric maps of NO_y on isentropic surfaces generated from CTM predict the NO_y mixing ratio to be rather uniform near Kiruna. On the other hand, NO_x and NO mixing ratios have large spatial variability near the terminator, where Kiruna was located.

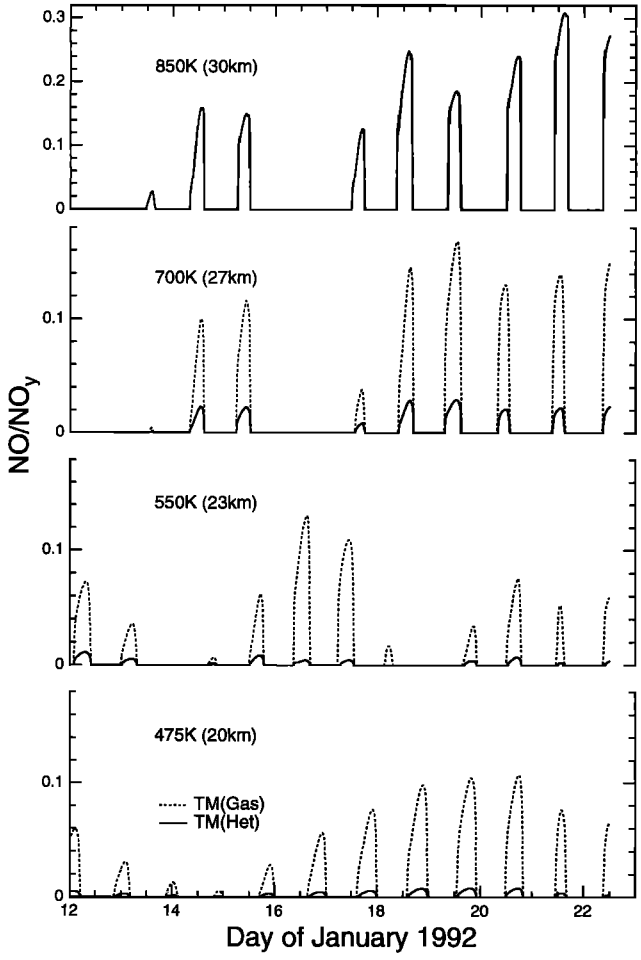

Figure 9. Temporal variation of the NO/NO_y ratio calculated by TM2 on four isentropic levels: 850, 700, 550, and 475 K.

The N_2O profiles calculated by CTM for January 22 and 31 are in good agreement with those observed below 22 km. At higher altitudes the model N_2O values are considerably higher than those measured, since the effect of strong descent by diabatic cooling in the Arctic winter is not well reproduced in the assimilation wind fields. On the other hand, the model NO_y values are in good agreement with those measured up to 30.5 km, giving a good basis for comparing the model and measurement for NO, since NO is determined by the partitioning among NO_y species.

The NO profiles calculated by CTM, TM1, and TM2 are in agreement with the observed profile between 20 and 27 km. The calculated NO values between 20 and 22 km are lower than 40 pptv, in agreement with the descent data. At this level, NO_x constitutes a very small fraction of NO_y. Reaction (R2), which is saturated already at SA of 1–2 μm^2 cm^{-3}, reduces the NO_x level by more than an order of magnitude. The increase in NO and the NO_x/NO_y ratio between 24 and 29 km results from the reduced SA and increased rate of generation of NO_x from HNO_3. The good agreement between the observations and TM1 results extends up to 30 km, owing mainly to the higher vertical resolution of TM1.

The CTM model predicts some diurnal variation of NO and NO_x in the morning. At 24 km the NO_x mixing ratio is 80 pptv at 0900 UT, while it is 270 pptv at 1200 UT. Considering the time constant of the photolysis of the reservoir species, the diurnal variation of NO_x results primarily from the $ClONO_2$ photolysis.

It has been found that the heterogeneous reaction (R2) can play a role in reducing NO at this altitude if SA of 0.04 μm^2 cm^{-3} is assumed. The present calculations, which do not include (R2) above 28 km, may overestimate NO values to some extent.

It can be concluded that CTM, TM1, and TM2 can generate the very low NO/NO_y ratios observed near the terminator where NO/NO_y ratios have large spatial variations. These models indicate that the NO/NO_y ratios were low for two main reasons: (1) There was very little sunlight to generate NO_x from HNO_3, and (2) there was oxidation of NO_x due to hydrolysis of N_2O_5 which was particularly noticeable between 20 and 23 km. The quantitative agreement between observed and model NO values indicates that photochemical and transport processes near the terminator and the vortex edge are accurately calculated by the models.

Acknowledgments. Partial funding by CEC and the Japanese MESC are gratefully acknowledged. Thanks are due to C. Schiller,

who showed us his data before publication. Potential vorticity maps were calculated by ECMWF and provided through NILU.

References

Aimedieu, P., Y. Kondo, T. Sugita, M. Koike, and W. R. Sheldon, In situ measurements of nitric oxide, ozone, and aerosol in the Scandinavian Arctic stratosphere in January 1992, *Geophys. Res. Lett.*, *21*, 1243–1246, 1994.

Anderson, D. E., The troposphere to stratosphere radiation field at twilight: A spherical model, *Planet. Space Sci.*, *31*, 1517–1523, 1983.

Anderson, D. E., Jr., and S. A. Lloyd, Polar twilight UV-visible radiation field: Perturbations due to multiple scattering, ozone depletion, stratospheric clouds, and surface albedo, *J. Geophys. Res.*, *95*, 7429–7434, 1990.

Anderson, D. E., Jr., R. DeMajistre, and S. A. Lloyd, Impact of aerosols and clouds on the troposphere and stratosphere radiation field with application to twilight photochemistry at 20 km, *J. Geophys. Res.*, *100*, 7135–7145, 1995.

Atkinson, R., D. L. Baulch, R. A. Cox, R. F. Hampson, J. A. Kerr, J. Troe, Evaluated kinetic and photochemical data for atmospheric chemistry, suppl. IV, IUPAC subcommittee on gas kinetic data evaluation for atmospheric chemistry, *J. Phys. Chem. Ref. Data*, *21*, 1125–1568, 1992.

Bauer, R., et al., Monitoring the vertical structure of the Arctic polar vortex over northern Scandinavia during EASOE: Regular N_2O profile observations, *Geophys. Res. Lett.*, *21*, 1211–1214, 1994.

Borrmann, S., et al., Aerosols as dynamical tracers in the lower stratosphere: Ozone versus aerosol correlation after the Mount Pinatubo eruption, *J. Geophys. Res.*, *100*, 11,147–11,156, 1995.

DeMore, W. B., et al., Chemical kinetics and photochemical data for use in stratospheric modelling, in *Evaluation 10, Tech. Rep. 92-20*, Jet Propul. Lab., Pasadena, Calif., 1992.

DeMore, W. B., et al., Chemical kinetics and photochemical data for use in stratospheric modelling, in *Evaluation 11, Tech. Rep. 94-26*, Jet Propul. Lab., Pasadena, Calif., 1994.

Deshler, T., In situ measurements of Pinatubo aerosol over Kiruna on four days between January 18 and February 13, 1992, *Geophys. Res. Lett.*, *21*, 1323–1326, 1994.

Evans, W. F. J., C. T. McElroy, and I. E. Galbally, The conversion of N_2O_5 to HNO_3 at high latitudes in winter, *Geophys. Res. Lett.*, *12*, 825–828, 1985.

Fahey, D. W., S. Solomon, S. R. Kawa, M. Loewenstein, J. R. Podolske, S. E. Strahan, and K. R. Chan, A diagnostic for denitrification in the winter polar stratosphere, *Nature*, *21*, 698–702, 1990.

Fahey, D. W., et al., In situ measurements constraining the role of sulphate aerosols in mid-latitude ozone depletion, *Nature*, *363*, 509–514, 1993.

Fried, A., B. E. Henry, and J. G. Calvert, The reaction probability of N_2O_5 with sulfuric acid aerosols at stratospheric temperatures and compositions, *J. Geophys. Res.*, *99*, 3517–3532, 1994.

Garcia, R. R., and S. Solomon, A new numerical model of the middle atmosphere, 2, Ozone and related species, *J. Geophys. Res.*, *99*, 12,937–12,951, 1994.

Hanson, D. R., and K. Mauersberger, Laboratory studies of the nitric acid trihydrate: Implications for the south polar stratosphere, *Geophys. Res. Lett.*, *15*, 855–858, 1988.

Hanson, D. R., and A. R. Ravishankara, The reaction probabilities of $ClONO_2$ and N_2O_5 on 40–75% sulfuric acid solutions, *J. Geophys. Res.*, *96*, 17,307–17,314, 1991.

Hanson, D. R., A. R. Ravishankara, and S. Solomon, Heterogeneous reactions in sulfuric acid aerosols: A framework for model calculations, *J. Geophys. Res.*, *99*, 3615–3629, 1994.

Harwood, R. S., and J. A. Pyle, Studies of the ozone budget using a zonal mean circulation model and linearised photochemistry, *Q. J. R. Meteorol. Soc.*, *103*, 319–343, 1977.

Harwood, R. S., and J. A. Pyle, The dynamical behaviour of a two-dimensional model of the stratosphere, *Q. J. R. Meteorol. Soc.*, *106*, 395–420, 1980.

Kawa, S. R., D. W. Fahey, K. K. Kelly, J. E. Dye, D. Baumgardener, B. W. Gandrud, M. Loewenstein, G. V. Ferry, and K. R. Chan, The Arctic polar stratospheric cloud aerosol: Aircraft measurements of reactive nitrogen, total water, and particles, *J. Geophys. Res.*, *97*, 7925–7938, 1992.

Kawa, S. R., et al., Interpretation of NO_x/NO_y observations from AASE II using a model of chemistry along trajectories, *Geophys. Res. Lett.*, *20*, 2507–2510, 1993.

Komhyr, W. D., R. A. Barnes, G. B. Brothers, J. A. Lathrop, and D. P. Opperman, Electrochemical concentration cell ozonesonde performance evaluation during STOIC 1989, *J. Geophys. Res.*, *100*, 9231–9244, 1995.

Kondo, Y., W. A. Matthews, P. Aimedieu, and D. E. Robbins, Diurnal variation of nitric oxide at 32 km: Measurements and interpretation, *J. Geophys. Res.*, *93*, 2451–2460, 1988.

Kondo, Y., N. Toriyama, W. A. Matthews, and P. Aimedieu, Calibration of the balloon-borne NO instrument, *J. Geomagn. Geoelectr.*, *41*, 507–523, 1989.

Kondo, Y., P. Aimedieu, W. A. Matthews, W. R. Sheldon, and J. R. Benbrook, A midlatitude balloon-borne observation of total odd nitrogen, *Geophys. Res. Lett.*, *17*, 73–76, 1990.

Kondo, Y., P. Aimedieu, M. Koike, Y. Iwasaka, P. A. Newman, U. Schmidt, W. A. Matthews, M. Hayashi, and W. R. Sheldon, Reactive nitrogen, ozone, and nitrate aerosols observed in the Arctic stratosphere in January 1990, *J. Geophys. Res.*, *97*, 13,025–13,038, 1992.

Kondo, Y., U. Schmidt, T. Sugita, P. Aimedieu, M. Koike, H. Ziereis, and Y. Iwasaka, Total reactive nitrogen, N_2O, and ozone in the winter Arctic stratosphere, *Geophys. Res. Lett.*, *21*, 1247–1250, 1994.

Lary, D. J., and J. A. Pyle, Diffuse radiation, twilight and photochemistry, *J. Atmos. Chem.*, *13*, 373–392, 1991.

Loewenstein, M., et al., New observations of the NO_y/N_2O correlation in the lower stratosphere, *Geophys. Res. Lett.*, *20*, 2531–2534, 1993.

Meier, R. R., D. E. Anderson, and M. Nicolet, The radiation field in the troposphere and stratosphere from 240 and 1000 nm: General analysis, *Planet. Space Sci.*, *30*, 923–933, 1982.

Mills, M. J., A. O. Langford, T. J. O'Leary, K. Arpag, H. L. Miller, M. H. Proffitt, R. W. Sanders, and S. Solomon, *Geophys. Res. Lett.*, *20*, 1187–1190, 1993.

Nash, E. R., P. A. Newman, J. R. Rosenfield, and M. R. Schoeberl, An objective determination of the polar vortex using Ertel's potential vorticity, *J. Geophys. Res.*, in press, 1996.

Nicolet, M., R. R. Meier, and D. E. Anderson, The radiation field in the troposphere and stratosphere from 240 to 1000 nm: Numerical analysis, *Planet. Space Sci.*, *30*, 935–983, 1982.

Ridley, B. A., et al., Stratospheric odd nitrogen: Measurements of HNO_3, NO, NO_2, and O_3 near 54°N in winter, *J. Geophys. Res.*, *89*, 4797–4820, 1984.

Ridley, B. A., M. McFarland, A. L. Schmeltekopf, M. H. Proffitt, D. L. Albritton, R. H. Winkler, and T. L. Thompson, Seasonal differences in the vertical distributions of NO, NO_2, and O_3 in the stratosphere near 50°N, *J. Geophys. Res.*, *92*, 11,919–11,929, 1987.

Schiller, C., A. Hofzumahaus, M. Müller, E. Klein, E.-P. Röth, and U. Schmidt, Ultraviolet actinic flux in the stratosphere: An overview of balloon-borne measurements during EASOE, 1991/1992, *Geophys. Res. Lett.*, *21*, 1239–1242, 1994.

Schubert, S. D., J. Pfaendtner, and R. Rood, An assimilated data set for Earth Science applications, *Bull. Am. Meteorol. Soc.*, *74*, 2331–2342, 1993.

Thomason, L. W., and L. R. Poole, Use of stratospheric aerosol properties as diagnostics of Antarctic vortex processes, *J. Geophys. Res.*, *98*, 23,003–23,012, 1993.

World Meteorological Organization, Scientific Assessment of Ozone Depletion: 1991, Global Ozone Research and Monitoring Project, *Rep. 25*, Geneva, 1992.

T. Deshler, Department of Atmospheric Science, University of Wyoming, Laramie, WY 82071.

A. R. Douglass and S. R. Kawa, NASA Goddard Space Flight Center, Code 916, Greenbelt, MD 20771.

M. Koike, Y. Kondo, and T. Sugita, Solar-Terrestrial Environment Laboratory, Nagoya University, Toyokawa, Aichi 442, Japan.

D. Lary and E. Lutman, Department of Chemistry, University of Cambridge, Lensfield Road, Cambridge CB2 1EW, England.

(Received September 12, 1995; revised January 31, 1996; accepted February 1, 1996.)